Research article

Wei Qi, Yu Yu* and Xinliang Zhang

On-chip arbitrary-mode spot size conversion

https://doi.org/10.1515/nanoph-2020-0328
Received June 11, 2020; accepted July 23, 2020; published online August 6, 2020

Abstract: Manipulating on-chip optical modes via components in analogy with free-space devices provides intuitional light control, and this concept has been adopted to implement single-lens–assisted spot size conversion using integrated device. However, the reported schemes have been demonstrated only for fundamental mode, while high-order or irregular modes are preferred in specific applications. The 4-f system is widely used in Fourier optics for optical information processing. Under the inspiration of the 4-f system and the beam expander in bulk optics, a spot size converter (SSC) with two metamaterial-based graded-index waveguides is proposed and demonstrated. The proposed device is capable of widening an arbitrary mode while preserving its profile shape. Compared with conventional SSC using adiabatic taper, the footprint can be reduced by 91.5% under a same intermode crosstalk. Experimentally, an expansion ratio of five is demonstrated for regular modes. Furthermore, for an irregular mode, the functionality is numerically verified without structure modification. This work offers a universal solution to on-chip spot size conversion and may broaden the on-chip application prospects of Fourier optics.

Keywords: integrated photonics; metamaterials; spot size conversion.

1 Introduction

On-chip photonic devices exhibit tremendous potentials in many applications, including communication, microwave photonic signal processing, quantum information, sensing and computing [1–6]. Recently, a novel design concept of manipulating on-chip modes as controlling free-space beams emerges. Using on-chip components in analogy with free-space devices, such as lenses, exhibits enormous advantages for intuitional control on trajectory and wavefront. For example, focusing lens has been adopted in fundamental-mode spot size converters (SSCs) [7–10]. Eaton lens has been demonstrated to bend the light trajectory on chip (waveguide bend) [11, 12], and Maxwell fish eye lens's aberration-free imaging property has been utilized to build multimode waveguide (MWG) crossings [13, 14]. Furthermore, fascinating functionalities of collimating on-chip Gaussian beams [15, 16], emulating curved spacetimes [17, 18], focusing with ultralow longitudinal spherical aberration [19] and optical diffractive computing [9] have also been implemented.

The 4-f system, consisting of two lenses, is a well-known system in Fourier optics. Instead of using bulk lenses, the functionality of this system can also be implemented by graded-index (GRIN) media [20, 21]. Although the optical information processing capability for these systems has been proved to be remarkable for computational applications, it can also inspire other unique functionalities demanded on a chip. For on-chip optical modes, the SSC is valuable both in intrachip and on/off-chip scenarios, and a compact SSC compatible with arbitrary modes can be regarded as a universal building block. For high-order modes (regular modes other than fundamental mode), spot size conversion is desired to fulfill the connection between multimode devices with different waveguide widths [22], and the coupling between few-mode fiber and chip [23, 24]. The reported schemes were based on the adiabatic mode evolution principle, lacking of compactness and/or compatibility with fundamental mode. Although nonadiabatic tapers and single-lens–assisted tapers are more compact, they have been demonstrated only for fundamental mode [7–10, 25, 26] and are difficult to accommodate high-order modes. Because of the inevitable excitation of other modes, nonadiabatic tapers need extra optimization for the compatibility with high-order modes. As for single-lens–assisted tapers, under the effect of the Fourier transform (FT) property of lens, the output mode profile is actually the input mode's spatial frequency spectrum. In high-order mode cases, the shape of this spectrum is normally different from that of the incident mode, resulting in the shape distortion. Transformation optics is another possible

*Corresponding author: Yu Yu, Wuhan National Laboratory for Optoelectronics, Huazhong University of Science and Technology, 1037 Luoyu Road, Wuhan 430074, China, E-mail: yuyu@mail.hust.edu.cn. https://orcid.org/0000-0002-8421-6794
Wei Qi and Xinliang Zhang, Wuhan National Laboratory for Optoelectronics and School of Optical and Electrical Information, Huazhong University of Science and Technology, Wuhan 430074, China

approach to achieve compact footprint [27], while the practical fabrication is complex. Moreover, the irregular modes were not considered yet, while the spot size conversion for them is also requisite. For instance, the irregular output mode for an on-chip diffractive computing system is measured by a waveguide array [9], whose scale is limited due to the waveguide width and separation to avoid crosstalk. Hence, the spatial resolution of measurement is restricted, and the spot size conversion to widen the irregular mode would be very helpful. To the best of our knowledge, on-chip SSCs for irregular modes have not been demonstrated. As a result, a compact and universal SSC for arbitrary modes is highly desired.

In this work, inspired by the 4-f system and the beam expander in bulk optics, we propose and demonstrate an on-chip arbitrary-mode SSC (AM-SSC) using the silicon-on-insulator (SOI) platform. Instead of utilizing conventional channel or ridge waveguides, two lens-like graded-index waveguide (GRINWG) using metamaterial are adopted. The working principle intuitively resembles that of the beam expander, while it can also be clearly interpreted in the perspective of Fourier optics. Similar to the 4-f system, this device works in a way of "optical image processing". The incident mode is treated as an "object", and an "image" with a different width is obtained at the output after the scaling caused by two consecutive FT operations. Owing to the fidelity in the "imaging" procedure, the profile shape of the incident mode ("object") is intrinsically preserved. With a footprint of $59.6 \times 25.5\ \mu m^2$, the AM-SSC widens an arbitrary-profile mode from 4 to 20 μm. As proof-of-concepts, both regular and irregular modes are investigated with transverse electric (TE) polarization. The length of the proposed device is 8.5% of conventional linear adiabatic taper with same performance. For two-TE-modes, a low intermode crosstalk is experimentally demonstrated. Furthermore, an irregular mode is numerically verified with <1 dB insertion loss (IL) over a 100-nm wavelength span.

2 Design and analysis

As a common bulk optical component, beam expander is widely adopted to collimate laser beam. It can be formed in a Keplerian telescope configuration (Figure 1A). In this configuration, there is an internal focus between two convex lenses (with focal lengths of f_1 and f_2). When a beam with a diameter D_i is incident, the output beam diameter D_o can be obtained via an expansion ratio of $D_o/D_i = f_2/f_1$ using ray optics analysis [28]. Here, an AM-SSC is proposed on the SOI platform (Figure 1B), consisting of two metamaterial-based GRINWGs (GRINWG1 and GRINWG2). A detailed view of the GRINWG is illustrated as the inset. The GRINWGs are of square law effective index distribution, and they can be regarded as the counterparts of two lenses, with lengths equal to the corresponding focal lengths (f_{GRINWG1} and f_{GRINWG2}). When the incident mode with width w_i propagating through the AM-SSC, it evolves into a wider mode with width w_o. Similar to the analysis in bulk optics, the expansion ratio M can be obtained as follow.

$$M = \frac{w_o}{w_i} = \frac{f_{\mathrm{GRINWG2}}}{f_{\mathrm{GRINWG1}}} \tag{1}$$

The effective index distribution of the GRINWG is defined as

$$n_{\mathrm{eff}}^2(y) = n_M^2\left(1 - g^2 y^2\right) \tag{2}$$

$$g = \frac{1}{w_{\mathrm{GRINWG}}/2}\sqrt{1 - \frac{n_m^2}{n_M^2}} \tag{3}$$

where g is a distribution parameter, n_M and n_m are the maximum and minimum effective indices in the distribution from center to edge, and w_{GRINWG} is the width of the GRINWG [29].

From the ray optics prospective [29], the focal length of the GRINWG can be estimated as

$$f_{\mathrm{GRINWG}} = \frac{\pi/2}{g} \tag{4}$$

It should be noted that from Equations (3) and (4), the f_{GRINWG} is inversely correlated with effective index ratio n_M/n_m. In view of minimizing the device size, a higher n_M/n_m is preferable. Meanwhile, the f_{GRINWG} is proportional to the w_{GRINWG}.

From the viewpoint of wave optics, if a mode propagates along the GRINWG for a distance of f_{GRINWG}, the FT is performed on it [20]. In this scenario, the AM-SSC can be analyzed using FT (see Supplementary Material). For an input mode profile $E_i(y)$, the output at the end of the GRINWG2 can be expressed as

$$E_o(y) \propto E_i\left(-\frac{f_{\mathrm{GRINWG1}}}{f_{\mathrm{GRINWG2}}}\, y\right) \tag{5}$$

This equation implies that, compared to the input mode, the output one is reversed and widened by a ratio $M = f_{\mathrm{GRINWG2}}/f_{\mathrm{GRINWG1}}$, with the profile shape $E_i(y)$ unchanged.

Based on the above analysis, an AM-SSC operating at 1550 nm is designed with expansion ratio $M = 5$. For each GRINWG, the cross-section is designed first, and then the focal length is evaluated in simulation. To implement the desired GRIN distribution, we firstly discretize the

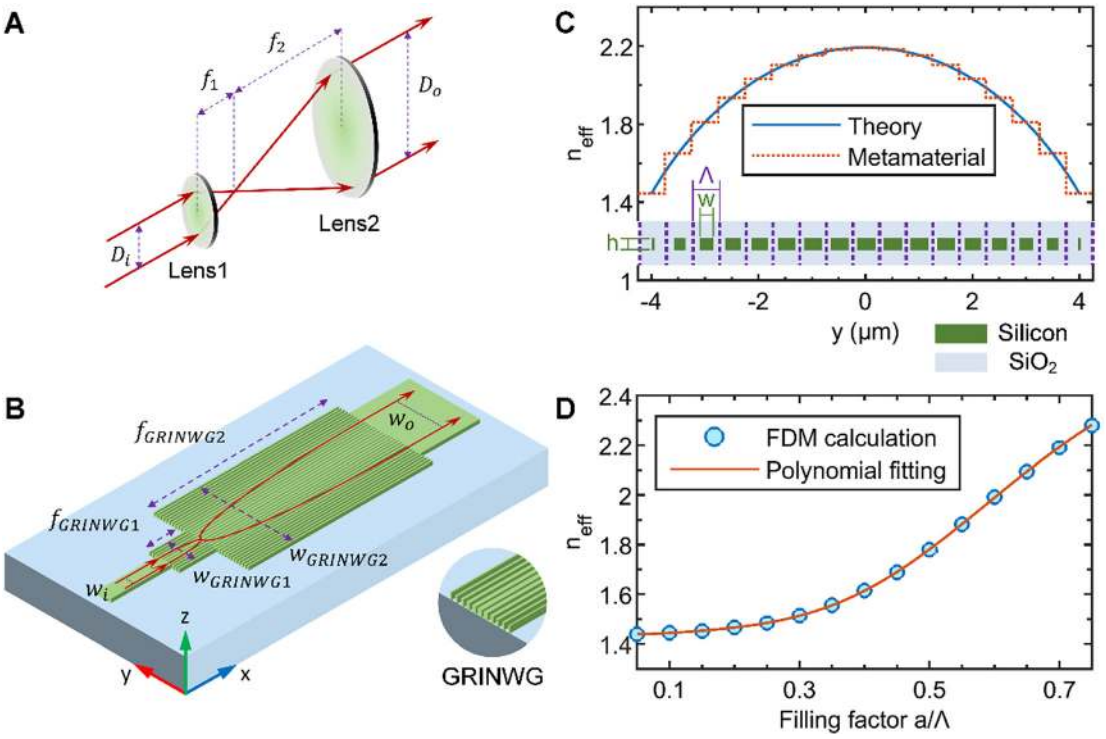

Figure 1: Schematic and the design of the proposed AM-SSC. (A) Beam expander in bulk optics. (B) On-chip AM-SSC consisting of two metamaterial-based GRINWGs. (C) Cross-section design of the GRINWG. (D) Element design library for metamaterial. SSCs, spot size converters; GRINWG, graded-index waveguide; AM, arbitrary mode.

distribution by period Λ (Figure 1C), and the cross-section is illustrated as the inset. Considering the fabrication feasibility, Λ is chosen to be 500 nm. The height of the metamaterial element (silicon nanostripe) is h = 220 nm, and a 2-μm-thick SiO_2 overcoating is used. By engineering the filling factor of the nanostripe element (defined as the ratio of element width w to period Λ), various effective indices n_{eff} can be achieved. The filling factor is set in the range of 0.1–0.7, corresponding to the effective index range of n_m = 1.44 to n_M = 2.19. As shown in Figure 1D, for the light with TE polarization, the effective index n_{eff} as a function of the filling factor is calculated via finite difference method (FDM). A design library for the metamaterial element is obtained by polynomial fitting of the FDM results. Then, the filling factor for each element (the width parameter of each nanostripe) is decided by consulting the library. For the determined cross-section, the focal length can be obtained by using the periodic self-focusing effect in the GRINWG, with a fundamental TE incident mode.

In the whole device, the GRINWG1 is firstly designed for effectively guiding the 4-μm-wide incident mode. Next, the GRINWG2 is designed straightforwardly by widening the GRINWG1's effective index distribution to obtain the desired focal length ratio. To be noted, a few elements on the edge of the two GRINWGs, which have little effect on the device performance, are neglected in the simulation and fabrication. The total footprint of the device is $59.6 \times 25.5\ \mu m^2$. Key parameters for the proposed device are summarized in Table 1.

To investigate the profile-shape-preserving property of the proposed AM-SSC, both regular and irregular modes are studied in simulation using eigenmode expansion method, with comparison to a single-lens SSC (SL-SSC). The SL-SSC contains only the GRINWG2 (identical to the one in the AM-SSC), and its principle is essentially the same as the reported single-lens–assisted tapers [7–10]. The light propagation inside the AM-SSC for three regular modes (TE_0, TE_1 and TE_2) are shown in Figure 2A, C and E, while

Table 1: Key parameters for the AM-SSC.

Parameter	GRINWG1	GRINWG2
Width (μm)	7.5	25.5
Length (focal length) (μm)	10	49.6
Period of nanostripe elements (nm)	500	500
Number of elements	15	51
Maximum element width (nm)	350	350
Minimum element width (nm)	213	290

SSC, spot size converter; AM, arbitrary mode; GRINWG, graded-index waveguide.

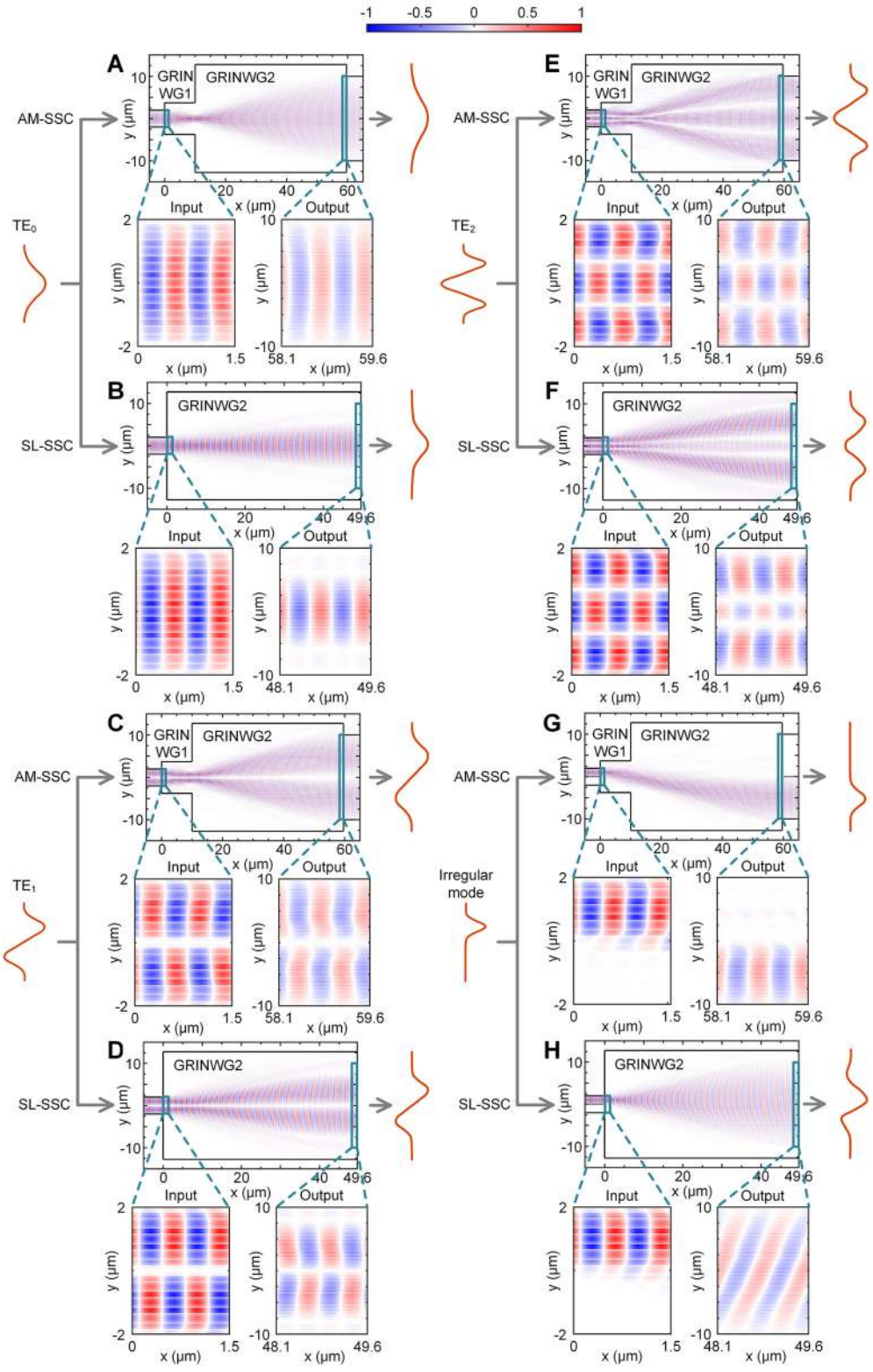

Figure 2: Light propagation profiles (E_y) inside the AM-SSC and the SL-SSC for various incident modes. Regarding to the AM-SSC, the profiles are calculated for (A) TE_0, (C) TE_1, (E) TE_2 and (G) irregular modes. For comparison, the results of the SL-SSC for these modes are also calculated in (B), (D), (F), and (H), respectively. Detailed profiles at the input and the output port are illustrated as insets. SSC, spot size converter; AM, arbitrary-mode; TE, transverse electric.

the case for an irregular mode is shown in Figure 2G. All the incident modes are 4 μm wide, while the irregular mode is asymmetrical in profile. The detailed profiles at the input and output ports are provided as insets. The profile shapes of the input and output modes are in good agreement (according to Equation (5), the output profile is reversed). Meanwhile, the expansion ratio is consistent for all the four modes. With regard to the SL-SSC, for the four incident modes identical to those investigated in the AM-SSC, the results are illustrated in Figure 2B, D, F and H, with detailed profiles showing as insets. On account of the single lens's FT property, the mode profile shape is not always preserved. For the TE_0 mode (on-chip Gaussian beam), the shape is preserved because the FT of Gaussian function remains Gaussian function, while this is normally not the case for high-order and irregular modes. The shape distortion is not obvious for the TE_1 mode, while easily observed for the TE_2 and the irregular mode. Besides, the expansion ratio varies among different modes. Being different from the SL-SSC, these results verify that, the AM-SSC widens various incident modes with "fidelity" (little distortion in profile shape) and a consistent expansion ratio.

In order to quantitatively evaluate the performance of the proposed device, the IL and intermode crosstalk (XT) are calculated in Figure 3. The intermode XT is defined as the power difference of any other mode and the incident mode. Because the GRINWG structure is symmetrical, the intermode XT between the symmetrical mode and the antisymmetrical mode is zero in theory. Hence, only the XT between TE_0 and TE_2 are investigated here. Results show that the ILs for the TE_0, TE_1 and TE_2 modes at 1550 nm are 0.03, 0.15 and 0.45 dB, respectively (Figure 3A–C). The values are lower than 0.5, 0.6 and 1 dB, over a 60-nm range from 1510 to 1570 nm. The intermode XT for the TE_0 and TE_2 incident modes are all <–20 dB over a 35-nm range in C-band. As for the irregular mode, the IL is 0.2 dB at 1550 nm, and <1 dB over 100 nm (Figure 3D). Thus, the proposed device is also compatible for irregular modes. In these results, minor fluctuations are observed due to the weak Fabry–Perrot resonance generated from the reflection between the channel waveguide and the GRINWG. The reflection can be reduced by increasing the effective index of the GRINWG. This could be implemented by increasing the maximum effective index (n_M) in the graded index profile. On the other hand, the intermode XT increases as the wavelength deviates from the central value because the focal length of GRINWG is sensitive to wavelength. The effective index of the GRINWG varies with wavelength, resulting in the variation of the focal length. A smaller period value (Λ) of the metamaterial element can be chosen to improve the dispersion [30].

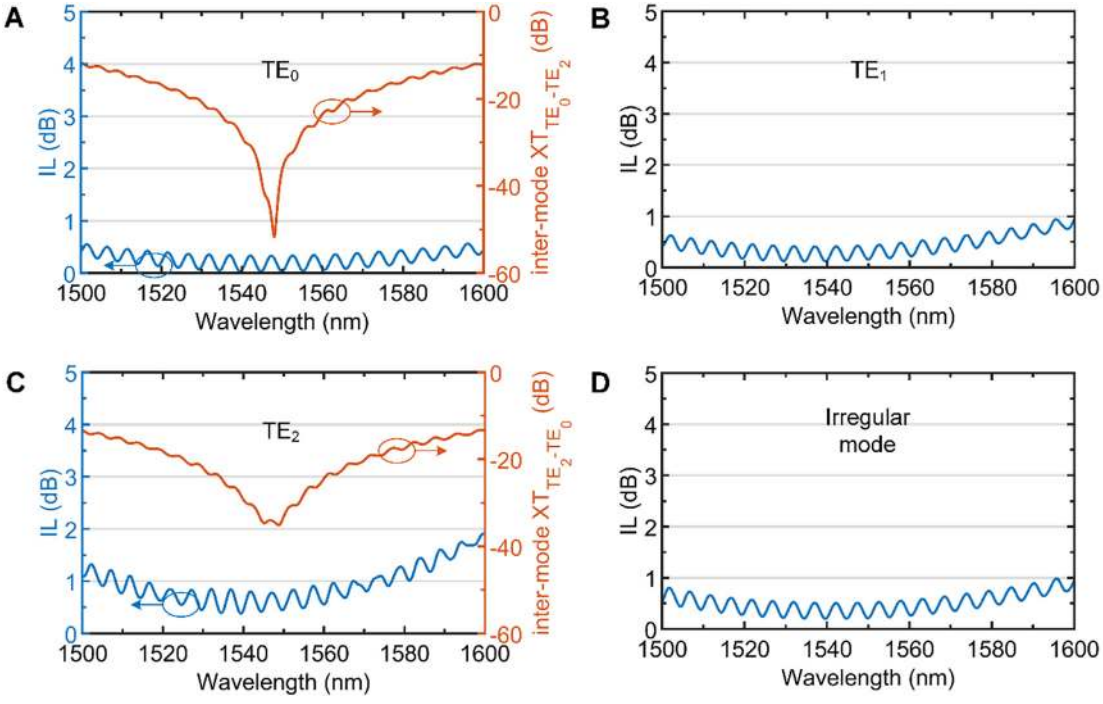

Figure 3: Insertion loss and intermode crosstalk spectra for the AM-SSC. The insertion loss values are calculated for (A) TE_0, (B) TE_1, (C) TE_2 and (D) irregular incident modes. The intermode crosstalk values are calculated for (A) TE_0 and (C) TE_2 incident modes. SSC, spot size converter; AM, arbitrary mode; TE, transverse electric.

In addition, for the functionality of regular modes' spot size conversion, conventional adiabatic tapers are usually fairly long due to the adiabatic condition [31]. For comparison, our simulation shows that a linear taper with width varying from 4 to 20 μm needs at least ~700 μm length to obtain <−20 dB intermode XT. For the proposed AM-SSC, the required length (59.6 μm) is 8.5% of the linear taper.

3 Fabrication and characterization

The proposed AM-SSC was fabricated and experimentally characterized for TE_0 and TE_1 modes. It was fabricated on the SOI platform with a 220 nm top silicon layer, using electron-beam lithography and inductively coupled plasma etching. A 2 μm top cladding layer of SiO_2 is deposited by plasma-enhanced chemical vapor deposition. Figure 4A presents the optical microscope image of the fabricated scheme, and the scanning electron microscope image of the GRINWG part is presented in Figure 4B. Grating couplers are applied for fiber-chip coupling. Two identical AM-SSCs (S1 and S2) are deployed in mirror symmetry to characterize the loss more precisely, with a connecting MWG. Both the width and length of the MWG are 20 μm. A pair of auxiliary two-TE-mode (de)multiplexers ((de)MUXer) is utilized to perform multiplexing and demultiplexing at the input and the output, respectively. The width transitions between the mode (de)MUXer and the AM-SSC are realized by adiabatic tapers to achieve minimized losses and intermode coupling. Via the S1, the input mode is widened from 4 to 20 μm. After propagating through the MWG, the widened mode is condensed back into 4 μm wide by the S2. Subsequently, it is demultiplexed into fundamental mode for characterization. Note that the 20-μm-wide MWG is placed here as an intermediate to verify that the width of the widened mode is 20 μm, considering the fact that any mode mismatch will result in intermode XT if the widened mode deviates from the designed dimension. Moreover, a reference link containing only mode (de)MUXers connected by an MWG was also

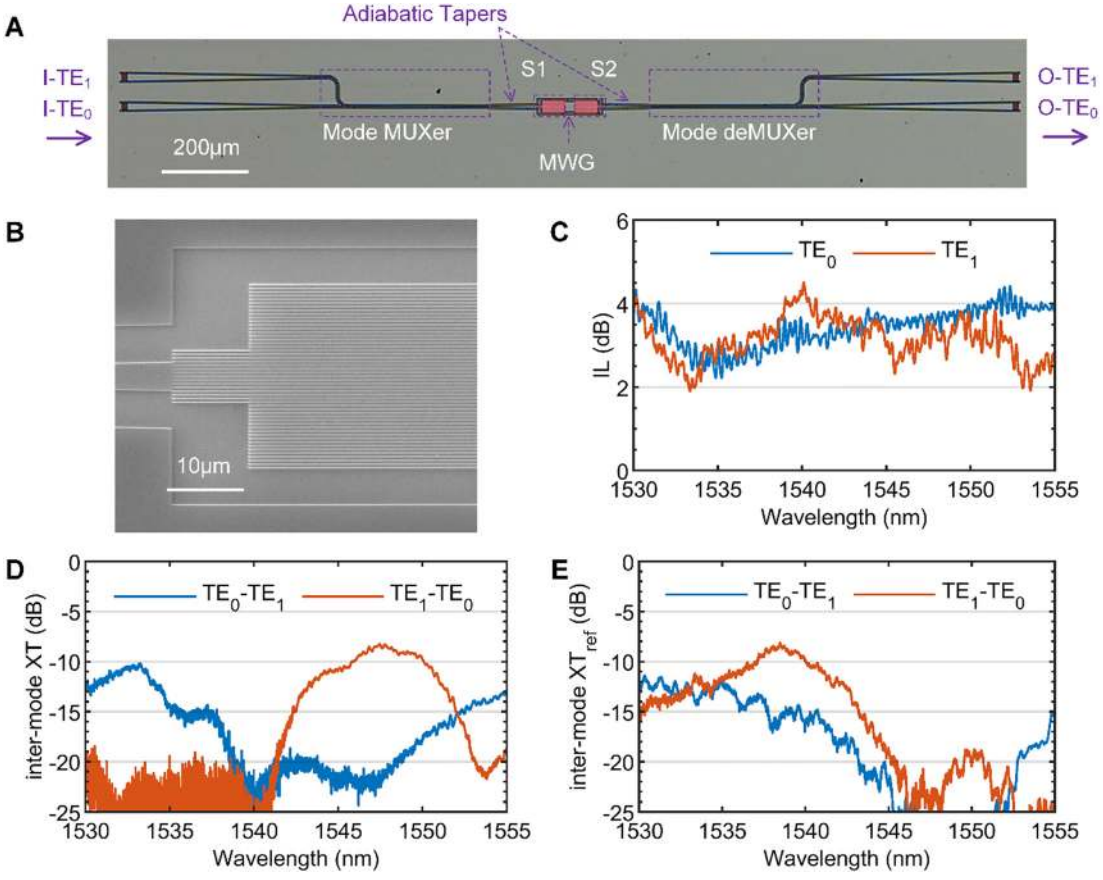

Figure 4: Device fabrication and characterization for the TE_0 and TE_1 modes. (A) Optical microscope image of the fabricated scheme. (B) SEM image of the GRINWG part. (C) Measured insertion loss spectra for TE_0 and TE_1 incident modes. (D) Measured intermode crosstalk spectra for TE_0 and TE_1 incident modes. (E) Measured intermode crosstalk spectra for TE_0 and TE_1 incident modes in the reference mode (de)MUXer link. GRINWG, graded-index waveguide; TE, transverse electric; SEM, scanning electron microscope.

fabricated for loss normalization and intermode XT comparison.

In the characterization, the light from a broadband source is sent to a polarization beam splitter to be linear polarized. A polarization controller is then adopted to maximize the coupling efficiency. The normalized IL and intermode XT spectra are shown in Figure 4C, D. Results show that the ILs for both two incident modes are ~3 dB from 1530 to 1555 nm, corresponding to an average IL of ~1.5 dB for each AM-SSC. Higher ILs in measurement compared with the simulation are probably attributed to the sidewall roughness and depth deviation in etching process. The intermode XT values are <−20 dB at 1540 nm for two incident modes. Across the span from 1530 to 1555 nm, the intermode XT values for TE_0 and TE_1 incident modes are <−7 dB. For comparison, the intermode XT spectra of the reference mode (de)MUXer link are provided in Figure 4E. The intermode XT values for two incident modes are also at the level of −7 dB, which indicates that the measured XT levels of the pair of AM-SSCs and the reference mode (de)MUXer link are similar.

4 Conclusion

We propose and demonstrate an on-chip AM-SSC in analogy with the 4-f system and the beam expander in bulk optics. It is able to widen an arbitrary mode from 4 to 20 μm with a compact footprint. Based on the working principle of Fourier optics, the device features a profile-shape-preserving property, and it is verified in simulation and experiment. This work may pave the way for on-chip photonic devices based on Fourier optics with diverse functionalities, and holds potentials for the applications including mode-division multiplexing systems, fiber-chip mode coupling and irregular mode profile measurement.

Acknowledgment: This work was supported by National Key Research and Development Program of China (2019YFB1803801, 2019YFB2203502), National Natural Science Foundation of China (61775073, 61922034), and Program for HUST Academic Frontier Youth Team (2018QYTD08).

Author contribution: All the authors have accepted responsibility for the entire content of this submitted manuscript and approved submission.

Research funding: This work was supported by National Key Research and Development Program of China (2019YFB1803801, 2019YFB2203502), National Natural Science Foundation of China (61775073, 61922034), and Program for HUST Academic Frontier Youth Team (2018QYTD08).

Conflict of interest statement: The authors declare no conflicts of interest regarding this article.

References

[1] A. H. Atabaki, S. Moazeni, F. Pavanello, et al., "Integrating photonics with silicon nanoelectronics for the next generation of systems on a chip," *Nature*, vol. 556, pp. 349–354, 2018.

[2] X. Zou, F. Zou, Z. Cao, et al., "A multifunctional photonic integrated circuit for diverse microwave signal generation, transmission, and processing," *Laser Photonics Rev.*, vol. 13, p. 1800240, 2019.

[3] S. Paesani, Y. Ding, R. Santagati, et al., "Generation and sampling of quantum states of light in a silicon chip," *Nat. Phys.*, vol. 15, pp. 925–929, 2019.

[4] C. V. Poulton, M. J. Byrd, P. Russo, et al., "Long-range LiDAR and free-space data communication with high-performance optical phased arrays," *IEEE J. Sel. Top. Quantum Electron.*, vol. 25, pp. 1–8, 2019.

[5] Z. Yan, G. Yerun, Q. Shiyu, et al., "Broadband multi-wavelength optical sensing based on photothermal effect of 2D MXene films," *Nanophotonics*, vol. 9, pp. 123–31, 2019.

[6] Y. Shen, N. C. Harris, S. Skirlo, et al., "Deep learning with coherent nanophotonic circuits," *Nat. Photonics*, vol. 11, p. 441, 2017.

[7] K. V. Acoleyen and R. Baets, "Compact lens-assisted focusing tapers fabricated on silicon-on-insulator," in *8th IEEE International Conference on Group IV Photonics*, Piscataway, IEEE, 2011, pp. 157–9.

[8] J. Zhang, J. Yang, H. Xin, J. Huang, D. Chen, and Z. Zhaojian, "Ultrashort and efficient adiabatic waveguide taper based on thin flat focusing lenses," *Opt. Express*, vol. 25, pp. 19894–19903, 2017.

[9] Z. Wang, T. Li, A. Soman, D. Mao, T. Kananen, and T. Gu, "On-chip wavefront shaping with dielectric metasurface," *Nat. Commun.*, vol. 10, p. 3547, 2019.

[10] J. M. Luque-González, R. Halir, J. G. Wangüemert-Pérez, et al., "An ultracompact GRIN-lens-based spot size converter using subwavelength grating metamaterials," *Laser Photonics Rev.*, vol. p. 13, p. 1900172, 2019.

[11] S. Hadi Badri and M. M. Gilarlue, "Low-index-contrast waveguide bend based on truncated Eaton lens implemented by graded photonic crystals," *J. Opt. Soc. Am. B*, vol. 36, pp. 1288–1293, 2019.

[12] S. Hadi Badri, H. Rasooli Saghai, and H. Soofi, "Polymer multimode waveguide bend based on a multilayered Eaton lens," *Appl. Opt.*, vol. 58, pp. 5219–5224, 2019.

[13] H. Xu and Y. Shi, "Metamaterial-based maxwell's fisheye lens for multimode waveguide crossing," *Laser Photonics Rev.*, vol. 12, p. 1800094, 2018.

[14] S. Li, Y. Zhou, J. Dong, et al., "Universal multimode waveguide crossing based on transformation optics," *Optica*, vol. 5, pp. 1549–56, 2018.

[15] U. Levy, M. Abashin, K. Ikeda, A. Krishnamoorthy, J. Cunningham, and Y. Fainman, "Inhomogenous dielectric metamaterials with space-variant polarizability," *Phys. Rev. Lett.*, vol. 98, p. 243901, 2007.

[16] G. Ren, T. G. Nguyen, and A. Mitchell, "Gaussian beams on a silicon-on-insulator chip using integrated optical lenses," *IEEE Photon. Technol. Lett.*, vol. 26, 1438–1441, 2014.

[17] C. Sheng, H. Liu, Y. Wang, S. N. Zhu, and D. A. Genov, "Trapping light by mimicking gravitational lensing," *Nat. Photonics*, vol. 7, pp. 902–6, 2013.
[18] C. Sheng, R. Bekenstein, H. Liu, S. Zhu, and M. Segev, "Wavefront shaping through emulated curved space in waveguide settings," *Nat. Commun.*, vol. 7, p. 10747, 2016.
[19] X.-T. He, Z.-Z. Huang, M.-L. Chang, et al., "Realization of zero-refractive-index lens with ultralow spherical aberration," *ACS Photonics*, vol. 3, pp. 2262–2267, 2016.
[20] D. Mendlovic and H. M. Ozaktas, "Fractional Fourier transforms and their optical implementation: I," *J. Opt. Soc. Am. A*, vol. 10, pp. 1875–1881, 1993.
[21] A. Silva, F. Monticone, G. Castaldi, V. Galdi, A. Alù, and N. Engheta, "Performing mathematical operations with metamaterials," *Science*, vol. 343, pp. 160–3, 2014.
[22] C. Sun, Y. Yu, Y. Ding, Z. Li, W. Qi, and X. Zhang, "Integrated mode-transparent polarization beam splitter supporting thirteen data channels," *Photonics Res.*, vol. 8, pp. 978–985, 2020.
[23] Y. Lai, Y. Yu, S. Fu, J. Xu, P. P. Shum, and X. Zhang, "Efficient spot size converter for higher-order mode fiber-chip coupling," *Opt. Lett.*, vol. 42, pp. 3702–3705, 2017.
[24] Y. Lai, Y. Yu, S. Fu, J. Xu, P. P. Shum, and X. Zhang, "Compact double-part grating coupler for higher-order mode coupling," *Opt. Lett.*, vol. 43, pp. 3172–3175, 2018.
[25] J. Zou, Y. Yu, M. Ye, et al., "Short and efficient mode-size converter designed by segmented-stepwise method," *Opt. Lett.*, vol. 39, pp. 6273–6276, 2014.
[26] P. Sethi, R. Kallega, A. Haldar, and S. K. Selvaraja, "Compact broadband low-loss taper for coupling to a silicon nitride photonic wire," *Opt. Lett.*, vol. 43, pp. 3433–3436, 2018.
[27] Q. Wu, J. P. Turpin, and D. H. Werner, "Integrated photonic systems based on transformation optics enabled gradient index devices," *Light Sci. Appl.*, vol. 1, p. e38, 2012.
[28] J. E. Greivenkamp, *Field Guide to Geometrical Optics*, Bellingham, SPIE Press, 2004.
[29] B. E. Saleh and M. C. Teich, *Fundamentals of Photonics*, Hoboken, John Wiley & Sons, 2007.
[30] R. Halir, A. Ortega-Moñux, D. Benedikovic, et al., "Subwavelength-grating metamaterial structures for silicon photonic devices," *Proc. IEEE*, vol. 106, pp. 2144–2157, 2018.
[31] Y. Fu, T. Ye, W. Tang, and T. Chu, "Efficient adiabatic silicon-on-insulator waveguide taper," *Photonics Res.*, vol. 2, pp. A41–A44, 2014.

Supplementary Material: The online version of this article offers supplementary material (https://doi.org/10.1515/nanoph-2020-0328).